High resolution electron microscopy of the triply incommensurate phase of $2H$-$TaSe_2$

Takashi Onozuka,* Nobuo Otsuka, and Hiroshi Sato
School of Materials Engineering, Purdue University, West Lafayette, Indiana 47907
(Received 12 December 1985; revised manuscript received 15 May 1986)

The triply incommensurate phase of $2H$-$TaSe_2$ obtained by cooling from the normal phase was investigated by transmission electron microscopy between 87 and 113 K with the resolution of 3 Å, one order of magnitude better than earlier experiments. Moirélike patterns observed in this phase were confirmed to be interference fringes due to the first- and second-order diffraction beams (with small separation and possibly with higher-order diffraction beams) from the incommensurate structure and were not due to the dark-field diffraction contrast of domains of the commensurate structure as interpreted earlier. Lattice fringes (~ 9 Å) of this modulated phase do not show any discontinuity across the boundaries of regions of different contrasts of the moirélike fringes which is expected from domain boundaries. Instead, a periodic change in the spacing of the lattice fringes (phase-slip region) expected from the superposition of split superlattice spots in forming the lattice image is observed. This is what is believed to be the first direct observation of the existence of the phase-slip region which is also expected from the discommensuration theory. A series of observations presented here thus shows that the triply incommensurate phase is intrinsically incommensurate and suggests the need for a modification of interpretations of this phase in terms of the double honeycomb discommensuration model.

INTRODUCTION

Along with long-period superlattices (LPS's) in alloys with a close-packed structure,[1-6] some transition-metal chalcogenides exhibit striking charge-density-wave (CDW) superlattice effects. Among others, $2H$-$TaSe_2$ exhibits a rich diversity of CDW superlattice phenomena including transitions between fully commensurate, incommensurate, and normal structures.[7] The present study concerns the triply incommensurate phase which is obtained by cooling from the normal phase. Below this temperature range, there exists an intermediate transition range between the commensurate phase and the incommensurate phase. In this transition range, the behavior strongly depends on whether the state is reached by cooling from the normal structure (above ~ 120 K) or by heating from the commensurate structure (below ~ 80 K). Electron microscopy studies of this "incommensurate phase" have been reported by Fung *et al.*[8] and by Chen *et al.*[9,10] among others.

Dark-field observations of this phase by means of the superlattice reflection exhibit moirélike fringes similar to those obtained from the superposition of two thin films. On the other hand, "stripe" patterns are observed in the transition region obtained by heating from the commensurate phase[8-10] and are found to change continuously to moirélike fringes by heating[8-10] These "stripe" patterns had been confirmed, by the dark-field imaging technique, to consist of domains of different orientations.[8,10] In this connection, these moirélike fringes have also been interpreted to be due to domains of the commensurate structure of different orientations.[8,10] From this interpretation, the "double honeycomb" discommensuration model[8] has been proposed for the structure of the incommensurate phase. According to this model, the dark region of the moirélike fringes is a chain of one type of domain which does not contribute to the superlattice reflection used for imaging.[8] Some inconsistencies of this interpretation with experimental results have been ascribed to the lack of resolution in the transmission electron microscopy (TEM) images in earlier studies[8] (resolution of around 50 Å). Subsequently, a high-resolution TEM observation of commensurate $2H$-$TaSe_2$ at ~ 70 K was reported.[11,12] However, the observation was limited to that of the lattice image itself and no additional information concerning problems of the incommensurate phase was included. This was the reason why we repeated the study of the incommensurate phase with higher resolution to settle unsolved problems in the earlier studies. At this time, the high-resolution study is limited to the temperature range of 85 to 113 K, or the upper temperature range of the incommensurate phase obtained by cooling from the normal phase.

EXPERIMENTAL PROCEDURES

Single crystals of $2H$-$TaSe_2$ were grown by means of a vapor-transport technique using I_2 gas as a transport agent at the Central Material Preparation Facility of Purdue University. The starting $TaSe_2$ powders also were prepared in this facility by reacting Ta powder with Se at 900 °C, because commercially available $TaSe_2$ powder was not sufficiently pure. The crystals thus obtained were hexagonal platelets approximately 7 mm across and 1 mm thick. These crystals were cleaved along the basal plane and mounted on copper grids for observation. A JEM 200 CX electron microscope with a modified side-entry, low-temperature stage with a liquid-nitrogen reservoir was used. The electron microscope has a resolution limit of 3.0 Å at the Schertzer defocus (-977 Å) under axial illumination. Observations were made between 85–120 K

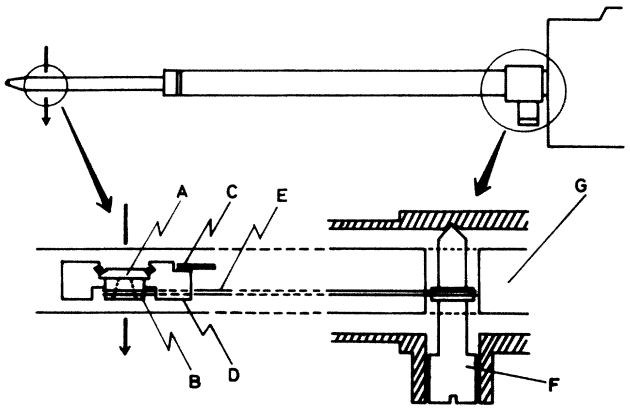

FIG. 1. Modified single-tilting, side-entry, liquid-N_2 stage with an additional rotation mechanism: *A*, specimen; *B*, rotation stage holder; *C*, copper conduction sheets; *D*, thermocouple; *E*, silk string; *F* rotation axis; *G*, conduction rod.

with the magnification of 20 000 to 200 000 times.

The modified stage was developed from a commercially available single-tilting stage, JEOL AM-SHTH, by adding a rotation mechanism as shown in Fig. 1 to provide the double-tilting function. The rotational motion was introduced by means of silk threads to isolate external motion from the stage when it was set. In order to avoid mechanical vibrations from the bubbling of the coolant, the liquid nitrogen was removed from the reservoir immediately before recording images. Because of the large heat capacity of the holder, several pictures could be taken before thermal drift of the specimen became appreciable. The minimum temperature attainable was determined by adjusting the number of copper conduction sheets used for controlling the conduction path and by evacuating the liquid-nitrogen tank. This method was essentially a modification of that used in the high-resolution observation of the Verwey transition in Fe_3O_4 at ~ 120 K.[13] By this method, however, the same resolution as that of ambient temperature could be obtained in the measurement between 87–113 K with the double-tilting stage. The measured temperature was that of the stage and the temperature of the specimen, being irradiated by the electron beam, was possibly higher by several degrees. In Fig. 2, the observation of the lattice fringes of ~ 3 Å of the background structure (the normal structure in the incommensurate phase) taken at 97 K with the low-temperature stage is shown.

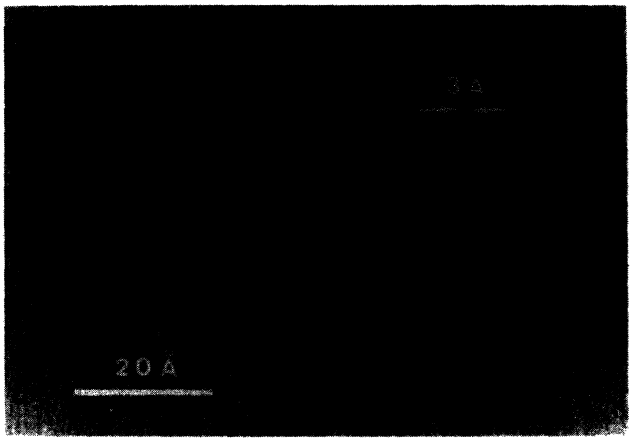

FIG. 2. High-resolution lattice images (spacing of ~ 3 Å) of the background normal structure at 97 K.

RESULTS

A typical diffraction pattern of the triply incommensurate phase taken at 97 K is shown in Fig. 3(a). The superlattice spots which correspond to the lattice modulation by CDW formation appear near the positions which divide the distance between two fundamental lattice reflections into three equal parts. Figure 3(b) shows enlargements of the region along the three major hexagonal axes between two fundamental reflections showing the splitting of each superlattice spot. This splitting is not recognizable on the screen of the microscope. Furthermore, this observation of split superlattice spots in previous TEM studies has never been reported. The split spots are a pair of spots with one spot of higher intensity than the other spot. The spot separation is approximately one hundredth of the distance between two fundamental lattice reflections, or approximately $(300\ \text{Å})^{-1}$. The existence of higher-order diffraction spots could not be detected.

The existence of these split spots has been observed in neutron diffraction experiments[14] and has been ascribed to

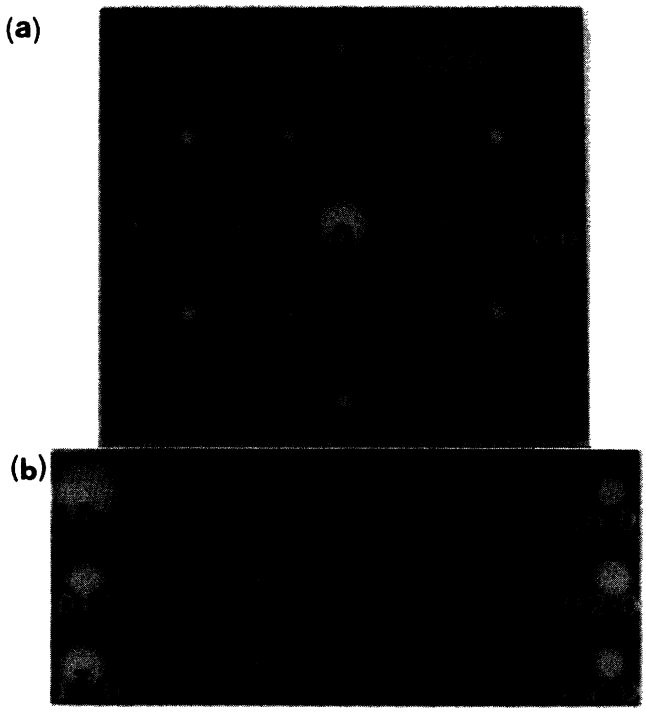

FIG. 3. (a) Electron diffraction pattern in the basal plane of $2H$-$TaSe_2$ at 97 K. The direction of the beam is parallel to the [00·1] direction. (b) Magnification of the above in three $[h\,0{\cdot}0]^*$ directions showing split superlattice spots (*P* and *S*).

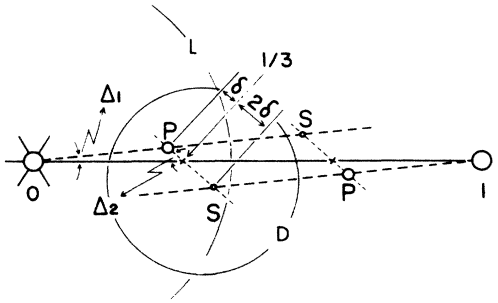

FIG. 4. Schematic representation of the diffraction pattern in one of the $[h0\cdot0]^*$ direction. The symbols 0 and 1 represent two fundamental diffraction spots and P and S represent the primary and the secondary superlattice diffraction spots, respectively.

the first-order and the second-order diffraction spots due to the lattice modulation created by CDW's. The appearance of the second-order spot is an indication that the lattice modulation is not perfectly sinusoidal, but a certain amount of the second-order harmonics is involved. In Fig. 4, a schematic representation of Fig. 3 in one direction is given for the convenience of later explanations. Here, the "incommensurability," δ, is defined as the deviation of the diffraction spot (primary peak P) from that for the commensurate phase (marked as $\frac{1}{3}$) (Refs. 14 and 15) with a period equal to three unit cells. The deviation of the secondary diffraction spot(s) from the $\frac{1}{3}$ position is then 2δ from the geometry.

The size of δ and the deviation (Δ_1) of the modulation vector ($\mathbf{Q}$) from the major hexagonal axis is shown exaggerated. The existence of nonzero Δ_1 is usually not detectable directly, and even if it exists, the deviation is limited to only one (or possibly two) direction(s) out of three major hexagonal axes as explained later. A nonzero value of Δ_1 indicates a deviation from hexagonal symmetry of the triply incommensurate phase. The deviation from hexagonal symmetry has never been reported in earlier studies. The value of δ is temperature dependent and was measured by both neutron[14] and x-ray[15] diffraction. The intensity of the secondary peak (S) is also highly temperature dependent and has been reported to vanish at around 115 K which is below the normal to incommensurate transition temperature of ~ 123 K.[14] The weakening of the intensity of the secondary spot with temperature is also clearly observed in the electron diffraction pattern in our experiment. The secondary diffraction spot with almost disappearing intensity along with the primary diffraction spot taken at 107 K (compare with that at 97 K) is shown in Fig. 5(b).

Dark-field images as shown in Fig. 6 utilize the superlattice diffraction beams contained in the circle D of Fig. 4 (the diameter is far larger than δ and, hence, higher-order diffraction beams, if any, can be included). These images exhibit parallel fringes reminiscent of moiré patterns derived from two overlapped thin films with slightly different lattice constants. Here, a set of the moirélike fringes at 97 K from the same area, but with three different $\mathbf{g}$ vectors (diffraction vectors) is shown. The locations of boundaries of the specimen at the left and the right corner of each micrograph show that these micrographs are from the same area. The low contrast in Fig. 6(c) is due to the fact that the secondary diffraction beam in this particular direction is not excited strongly at the orientation for these micrographs. Although somewhat irregular, the orientation of these stripes is always approximately perpendicular to the $\mathbf{g}$ vector used, and fringes in two or three simultaneous orientations for a particular $\mathbf{g}$ vector are never found. This type of set of photographs, although very important, has never been considered at this

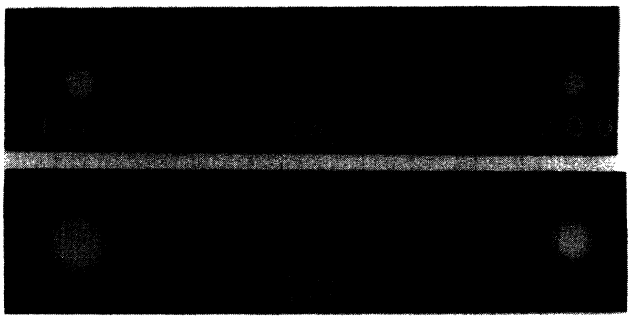

FIG. 5. Split superlattice spots at 107 K (b) as compared to those at 97 K (a). Note that S spot taken at 107 K (b) is almost invisible.

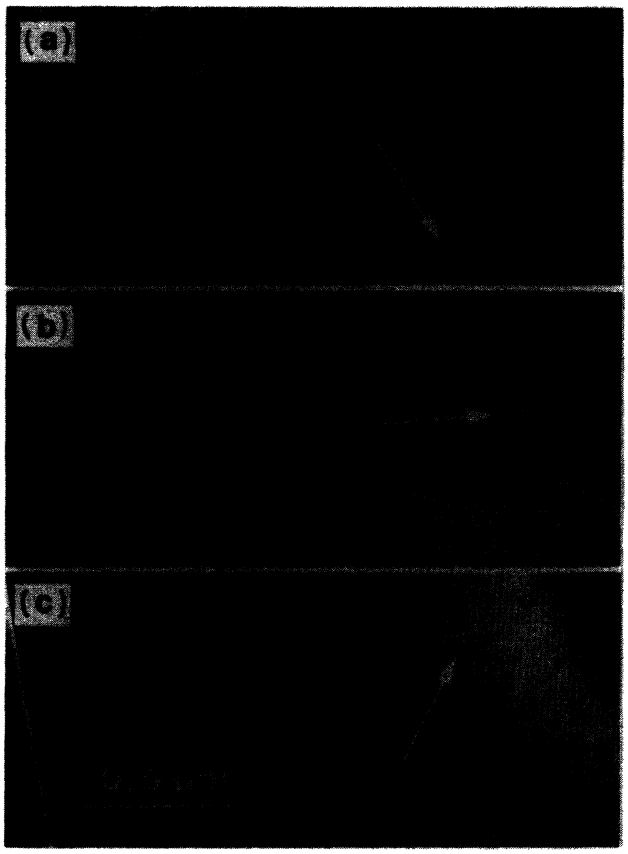

FIG. 6. Moirélike fringes obtained by the dark-field technique from the same area utilizing three different diffraction vectors, $\mathbf{g}$, taken at 97 K. Arrows indicate the directions of $\mathbf{g}$ of each micrograph.

temperature range because it had been thought technically difficult[10] based on the double honeycomb model.

In Fig. 7, the temperature change of the moirélike fringes with one **g** vector is shown. This figure shows that the spacing of the moirélike fringes is temperature dependent and decreases as the temperature becomes higher. These features are essentially the same as those observed by previous investigators in this temperature range.[8-10] However, for two of the three **g** vectors employed and one in particular, these fringes tend to deviate from the perpendicular orientation to the **g** vector as the temperature is lowered. At 87 K, the deviation amounts to as much as $\sim 20°$. This deviation is indicated in Fig. 4 as the angle Δ_2 or as $\Delta_1 \neq 0$. This tendency in the orientation of the moirélike fringes in this phase has not been noted previously.

The temperature dependence of the spacing of the moirélike fringes should be equal to $1/(3\delta)$ if the fringes are due to the interference from the two spots P and S.

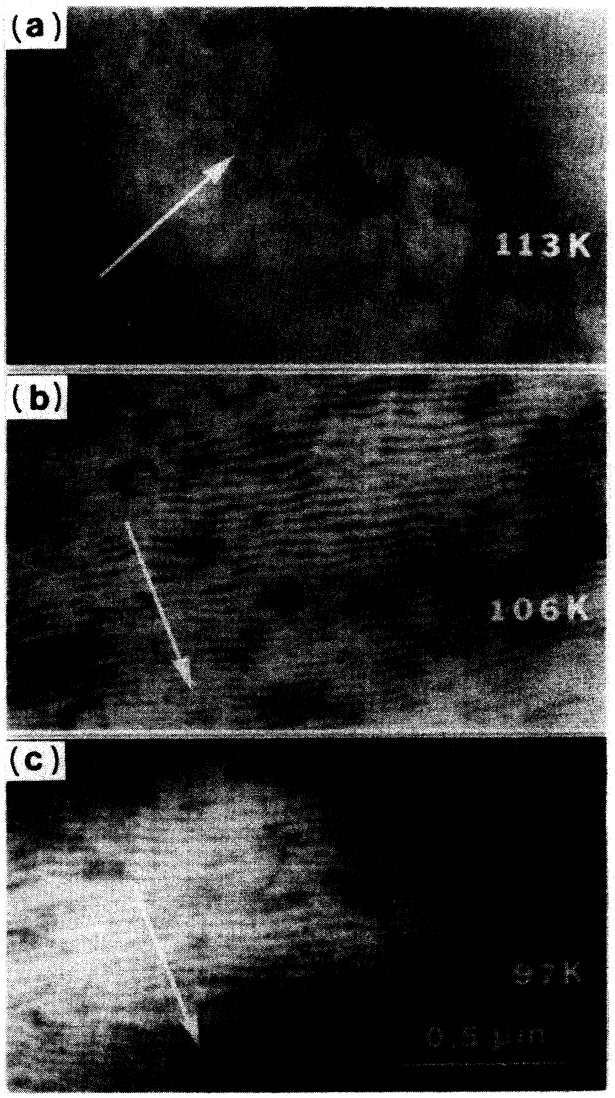

FIG. 7. Temperature dependence of the moirélike fringes. Arrows indicate the direction of the **g** vector. (a) 113 K, (b) 106 K, (c) 97 K.

The spacing of the stripes and $1/(3\delta)$ measured by x-ray[15] and neutron diffraction[14] are compared in Fig. 8. The agreement of the spacing of the moirélike patterns and the value $1/(3\delta)$ as shown in Fig. 8 has not been noted earlier. The spacing of the moirélike fringes is shifted towards the low-temperature side by about 5—7 K compared to $1/(3\delta)$ obtained by x-ray and neutron diffraction. This is because the temperature for the moirélike fringes is specified by that of the stage and, hence, this deviation indicates the difference between the temperature of the stage and that of the specimen. As the temperature rises, the intensity of the fringes decreases rapidly as well as the spacing, and at 133 K, the fringes become almost invisible at a spacing of approximately 130 Å. In other words, this decrease in intensity of the fringes is due to the decrease in the intensity of the secondary peak S as observed in Fig. 5, and, hence, the disappearance of the fringes is due to the disappearance of the secondary spot S and is not due to the fact that the spacing of the fringes becomes zero as indicated in earlier reports. Above this temperature, the lattice modulation is practically sinusoidal and is incommensurate with the incommensurability δ. All the features of the moirélike patterns in this phase are thus explained quite naturally as the interference of the primary (P) and secondary (S) (and possibly higher-order) diffraction beams indicated in Figs. 3 and 5. This observation is not consistent with the earlier interpretation that the fringes in this phase are due to dark-field diffraction contrast.[8]

The rotation of the moirélike fringes with respect to the diffraction vector (**g**) at lower temperatures (angle Δ_2) is due to a slight directional shift of the **Q** vector (angle Δ_1) as shown in Fig. 4. The rotation angle of fringes (Δ_2) is observed magnified (the moiré magnification Δ_2/Δ_1) because δ is small. In other words, this experiment clearly shows a slight deviation of the triply incommensurate phase from the hexagonal symmetry which had not been noted earlier. The wavy natures of the moirélike fringes is probably a local fluctuation of the **Q** vector due to strain or some other factors.

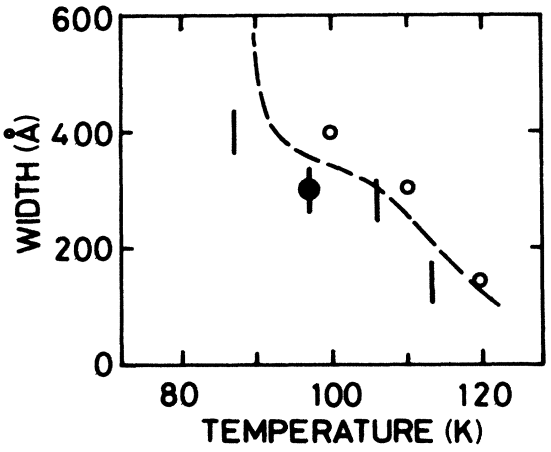

FIG. 8. Temperature dependence of the spacings of the moirélike fringes (shown by error bars and one with a solid circle) as compared to $1/(3\delta)$ measured by neutron diffraction (Ref. 15) (open circles) and x-ray diffraction (Ref. 16) (dashed line).

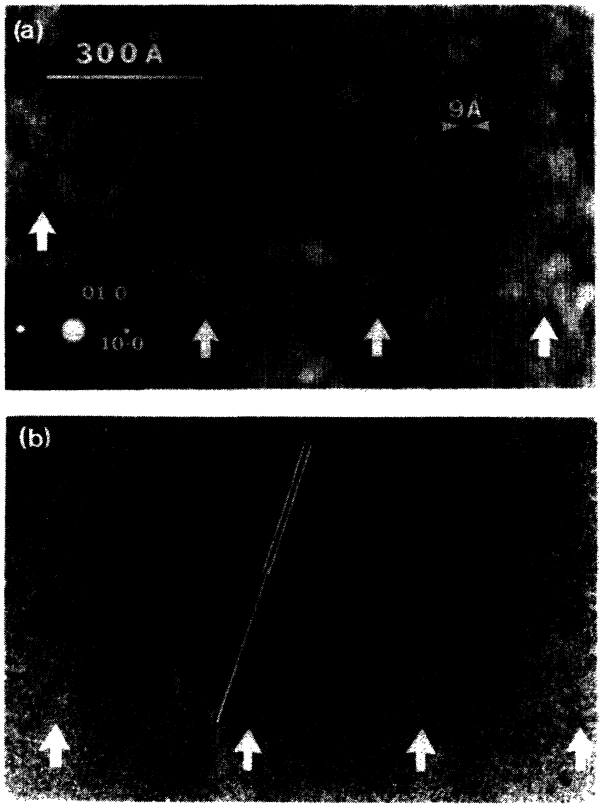

FIG. 9. High-resolution observation of CDW lattice fringes taken at 97 K. Areas of weaker contrast of lattice fringes (phase-slip region) are indicated by open arrows. (a) Lattice fringes are parallel to the phase-slip region (along with the corresponding diffraction pattern). (b) Lattice fringes are making $\sim 15°$ with respect to the phase-slip region.

Lattice fringes of the CDW phase were taken in axial illumination by including the area indicated by the circle L in Fig. 4, with a small tilt of the specimen along one of the **g** vectors so that superlattice diffractions along other **g** vectors were not excited in order to increase the intensity of the lattice images. Lattice fringes of the spacing of ~ 9 Å, which represents the period of the incommensurate phase, are observed perpendicular to the active **g** vector. The photograph taken at 97 K is shown in Fig. 9(a). Regions of weaker contrast of width of ~ 100 Å are also found to exist [shown by open arrows in Fig. 9(a)] with the period of ~ 300 Å which corresponds to the spacing of the moirélike fringes. Not only is the contrast low, the lattice images are less sharp in these regions. However, the spacing of the lattice fringes is more or less the same across the boundary between the areas of the two different contrasts and the lattice fringes are almost homogeneously visible over a wide area irrespective of the change of contrast. In other words, the lattice fringes do not show any sign of the existence of domains of different orientations. Furthermore, the lattice fringes do not show the extinction expected from the double honeycomb model.[8]

The moirélike fringes are not strictly parallel among themselves as pointed out earlier. Figure 9(b) shows the lattice fringes of ~ 9 Å from a region with $\Delta_2 \simeq 15°$. The regions of weak contrast of the lattice images which also corresponds to the dark region of the moirélike fringes are shown by open arrows. Again, a distinct change of contrast of the lattice fringes at the boundary which would indicate the existence of domains of different orientations is not observed.

A close scrutiny of high-resolution images of the CDW lattice fringes shown in Figs. 9(a) and 9(b), however, reveals some interesting features. In Fig. 10, the spacing of

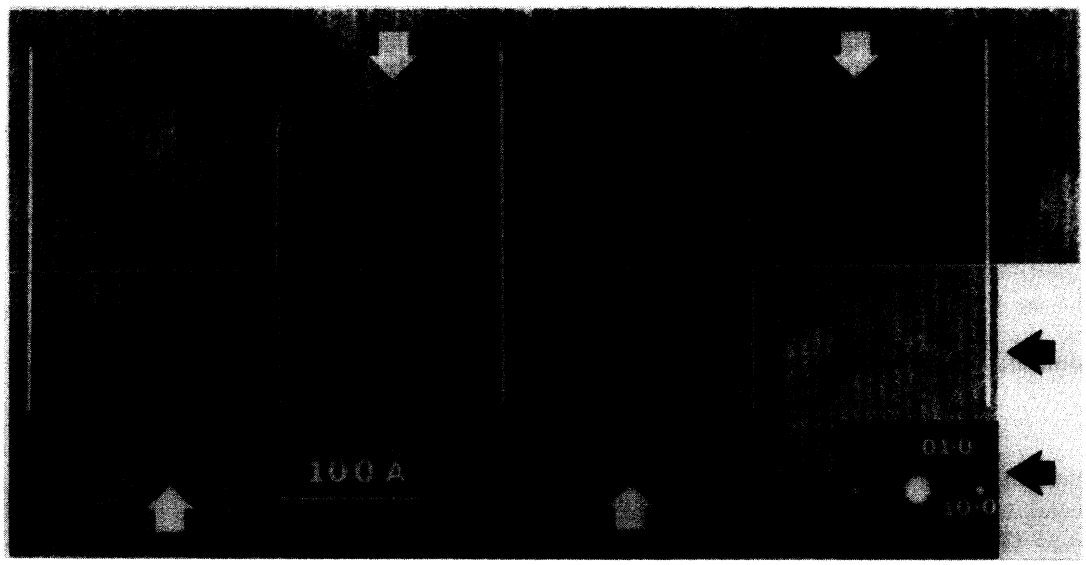

FIG. 10. Periodic change of CDW lattice spacings, showing the existence of the phase-slip region. The lower half of the picture is shifted to the left by approximately 150 Å along the solid arrows in order to compare the spacings of lattice fringes in the phase-slip region and in the other region.

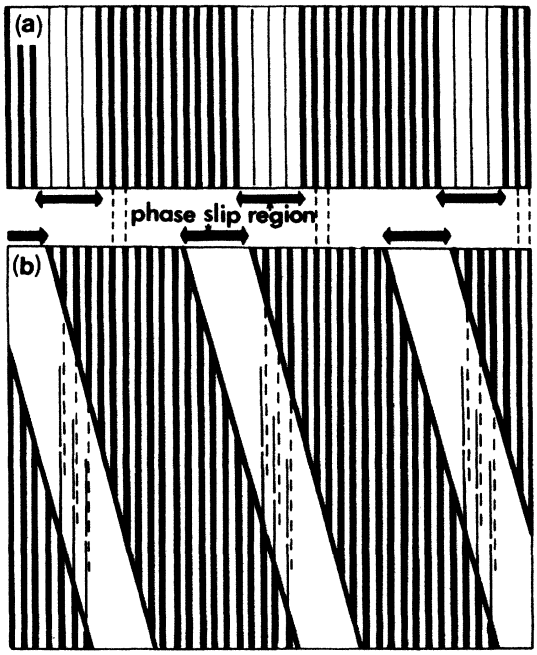

FIG. 11. Schematic view of the CDW lattice fringes with respect to the phase-slip region. In each case, the total phase shift in the position of lattice fringes across the phase-slip region is approximately $2\pi/3$. (a) The lattice fringes are parallel to the phase-slip region. (b) The lattice fringes make $\sim 15°$ with respect to the phase-slip region.

the lattice fringes in the area of the weaker contrast is compared with that in the area of the stronger contrast in the same figure by shifting the lower part of Fig. 9(a) in the direction of the black arrows by about 150 Å. This picture shows clearly that the spacing in the area of the weaker contrast is somewhat larger (by ~ 3 Å in 100 Å) than that in the stronger contrast area. This results in the phase shift of $\sim 2\pi/3$ across the region of weaker contrast. On the other hand, in Fig. 9(b), there seems to be a shift in the location of the fringes between two neighboring areas of the stronger contrast across an area of the weaker contrast which again corresponds to a phase shift of $\sim 2\pi/3$. This situation is shown schematically in Figs. 11(a) and 11(b). This type of phase shift in lattice images of $2\pi/3$ can be explained easily as a result of inclusion of the two split superlattice spots with separation of δ and 2δ around the position $\frac{1}{3}$ in the formation of the lattice images (see the Appendix). The region of the phase shift directly corresponds to the phase-slip region in the discommensuration theory[16,17] and is so indicated in Fig. 11.

SUMMARY AND DISCUSSION

Experimental data presented here are those in the temperature range of the triply incommensurate phase of $2H$-$TaSe_2$. Because of the hysteresis with respect to the incommensurate-commensurate transition, the discussion here is limited to the behavior of the phase obtained by cooling from the normal phase and in the temperature range near 100 K and above. The lowest specimen temperature attained was approximately 90 K (stage temperature ~ 85 K). High-resolution TEM observations which utilize split superlattice spots enabled us to obtain some illuminating information with respect to the nature of the triply incommensurate phase which had never been accessible.

A major feature of this phase is the appearance of the moirélike fringes as presented in Figs. 6 and 7 in a dark-field image utilizing superlattice diffraction beams (area D in Fig. 4). These fringes had been commonly interpreted to be the dark-field diffraction contrast based on the double honeycomb discommensuration model.[8] The double honeycomb discommensuration model is essentially an assembly of domains of the commensurate structure of the orthorhombic symmetry in the three different orientations to form a hexagonal symmetry with a phase shift of $2\pi/3$ between two adjacent domains of the same orientation. The dark contrast in the moirélike fringes is considered to represent the chain of domains of one orientation from which the diffraction beam is not excited.[8] However, in the present temperature range, images which indicate the chain of rhombus-shape domains expected from the double honeycomb model was never observed even with the resolution of 3 Å.

The idea that the appearance of the moirélike patterns is mainly due to the interference of split superlattice spots P and S is well supported by observations such as the spacing of the moirélike fringes which is equal to $1/(3\delta)$ (Fig. 8), the disappearance of the contrast of the fringes with the disappearance of the intensity of the spot S at higher temperatures [Fig. 5 and Fig. 6(a)], and the high-resolution electron micrographs of the CDW lattice fringes where the contrast due to the existence of boundaries of domains of different orientations is not observed [Figs. 9(a) and 9(b)]. The appearance of the two spots P and S ($\frac{1}{3}-\delta$ and $\frac{1}{3}+2\delta$) can also be explained by a domain model as being the incommensurate modulation of the commensurate structure somewhat similar to that in the long-period superlattice in alloys[1-6] with a phase shift of $2\pi/3$ at the domain boundaries such as in the double honeycomb model. However, in such a case, both split spots should be the first-order diffraction spots and, hence, no strong inequality in the temperature dependence in the intensity of the two spots P and S is expected as against that observed in Fig. 5. In addition, in a domain model such as the double honeycomb discommensuration model, the splitting of the commensurate spot, $\frac{1}{3}$, should be in three directions[8] rather than in the single direction as observed in Fig. 3(b). Splitting of the spot, $\frac{1}{3}$, in three directions has never been observed in the temperature range studied.

The appearance of the second-order diffraction spot S is due to the appearance of the second-order harmonic in the modulation mode of the lattice. Physically, this is an effort of the material to have the lattice modulation due to CDW formation in phase with the normal structure to lower the modulation free energy. Similar features have been observed in the long-period superlattice in alloys.[4-6] This change in the modulation mode can be either amplitude modulation or phase modulation, or both, depending

on the case.[3,14,16] One most conspicuous feature of $2H$-$TaSe_2$ is that the commensurate structure is relatively short (three normal unit cell lengths) and δ is small so that the second-order harmonic (S) appears close to the primary diffraction spot (P) at the location $\frac{1}{3}+2\delta$ against the first-order spot P at the location $\frac{1}{3}-\delta$ as shown in Fig. 4. This situation creates, in the dark-field image, the moirélike fringes of relatively large spacing, and in the high-resolution CDW lattice images (Figs. 9 and 10), the appearance of the phase-slip region with phase shift of $2\pi/3$ (see the Appendix). Higher-order harmonics can contribute to the image formation. For reference, the higher-order diffraction spots which might contribute to the high-resolution CDW images (Figs. 9 and 10) under the present experimental condition are shown in Fig. 12. If the scattering center is highly localized, higher-order harmonics of diffraction can arise from a purely sinusoidal modulation.[14] However, for a rather qualitative discussion of the TEM image contrast here, this contribution of the higher-order harmonics, the intensity being small,[14] does not seem to play an important role.

On the other hand, if the period of the commensurate phase is longer (four or five unit cell length, for example), the diffraction spot which would appear close to the primary spot, P, would be higher-order harmonics such as the third-order or the fourth-order spot and the intensity of such higher-order harmonics is expected to be weak. Therefore, interesting features observed in $2H$-$TaSe_2$ may not be expected in such cases unless the intensities of these higher-order spots are extremely high.

As mentioned earlier, the appearance of higher-order harmonics in the CDW diffraction spots is essentially an indication of the effort of materials to have the lattice modulation determined by the CDW formation in phase with the commensurate period or the background normal lattice to lower the modulation free energy. In order to achieve this effect, McMillan[16] superposed on the fundamental plane wave, which represents the CDW sinusoidal modulation P, a series of distortion waves (which eventually corresponds to the inclusion of higher harmonics whose major one is represented by S) in his treatment of discommensuration. Therefore, his treatment of discommensuration and especially that of Nakanishi and Shiba[17] who introduced the amplitude modulation as well as the phase modulation in the treatment, is essentially equivalent to our treatment of image formation of CDW lattice image by superposing P, S, and other possible higher-order harmonics (Appendix). In this sense, the observation of the "phase-slip" region in Figs. 9 and 10 corresponds to the existence of the phase-slip region in the intermediate temperature range in the discommensuration theory.[16,17] In other words, our high-resolution observation (Fig. 9) in the triple-Q phase represents a natural consequence of the discommensuration theory by McMillan[16] and Nakanishi *et al.*[17] The temperature dependence of the "phase-slip" region has been measured by Suits *et al.* by NMR (Ref. 18) and reported to be in agreement with the McMillan's hypothesis of discommensurations. Indeed, the data by Suits *et al.* also explains our high-resolution figures with $\gamma=0.01$, where γ gives essentially the measure of the width of the "phase-slip" region.[16,18]

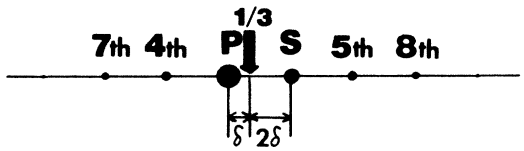

FIG. 12. Schematic representation of higher-order superlattice diffraction spots close to the commensurate point, $\frac{1}{3}$, in $TaSe_2$ which can contribute to the dark-field images as well as to the high-resolution lattice images.

The width of the "phase-slip" region tends to zero as the incommensurate-commensurate transition temperature is approached. However, we have not made observations at low enough temperatures such that a "phase-slip" region tends to an "out of step" boundary.

The phase shift across the "phase-slip" region (corresponds to the dark contrast area in moirélike fringes) in the present case amounts to $2\pi/3$. Therefore, it is easy to explain the characteristic patterns in the moirélike fringes in which three dark fringes terminate at one point (stripe or jelly-fish pattern with three legs) as shown in Fig. 13 [magnification of the moirélike fringes observed at 97 K (Fig. 6)]. In other words, it is not necessary to resort to the double honeycomb discommensuration model[8] to explain this characteristic pattern in moirélike fringes.

As the temperature is lowered the Q vector in two of the three hexagonal axes deviates slightly from the hexagonal directions ($\Delta_1\neq 0$) as observed from the rotation ($\Delta_2\neq 0$) of the moirélike fringes. This indicates the onset of at least the orthorhombic distortion of the triply incommensurate phase from the hexagonal symmetry, although an accurate determination of this effect is difficult based only on the micrographs (Fig. 8). If this distortion exceeds a certain limit, the triply incommensurate phase would split into domains of this distorted phase in three different orthorhombic directions in order to relieve the strain energy. This situation seems to explain the change of the moirélike fringes at high temperatures into those of domains at low temperatures. Although this changeover requires further investigation, at this stage the situation becomes extremely similar to the predictions from the double honeycomb discommensuration model, with the exception that the structure inside each domain is expected to be incommensurate rather than commensurate.

The accounts given here are logical consequences of our high-resolution observations of the so-called triply incommensurate phase in the temperature range around 100 K and above. It is clear that these observations support the fact that the triply incommensurate phase is intrinsically incommensurate and is not an incommensurate modulation of the commensurate structure. Also, the temperature dependence supports the discommensuration concept of McMillan *et al.*[16,17] On the other hand, the commonly accepted double honeycomb discommensuration model, although it is very ingenious and has some support in the temperature range close to the incommensurate-commensurate transition, seems to require some modifications at the high-temperature range. Additional evidence to support the present view will be published shortly.[19]

That the lattice modulation tends to be in phase with

the background normal lattice period and to take the commensurate period at lower temperatures is generally found in any modulated structure created by CDW formation.[1-6] The detailed behavior, however, depends on the mode of lattice modulation. In long-period superlattices in alloys such as CuAu II, an incommensurate modulation of the normal ordered structures (such as CuAu I) in terms of antiphase boundaries (instead of static phonons) appears. Because the antiphase modulation is intrinsically a commensurate, square-wave modulation unless the disordering of atoms at the boundary takes place, there exists complicated discommensuration phenomena especially when the modulation period is short.[5] Certain types of discommensuration phenomena in such alloys have been extensively investigated by one of the authors.[4-6] In these alloys, there exists a close analog to the discommensuration behavior of $TaSe_2$. The Ag-Mg alloys near Ag_3-Mg in which the average modulation period M is close to 2, for example, show interesting discommensuration behavior which is in parallel with the interpretations presented here. A part of this study will be published shortly.[20]

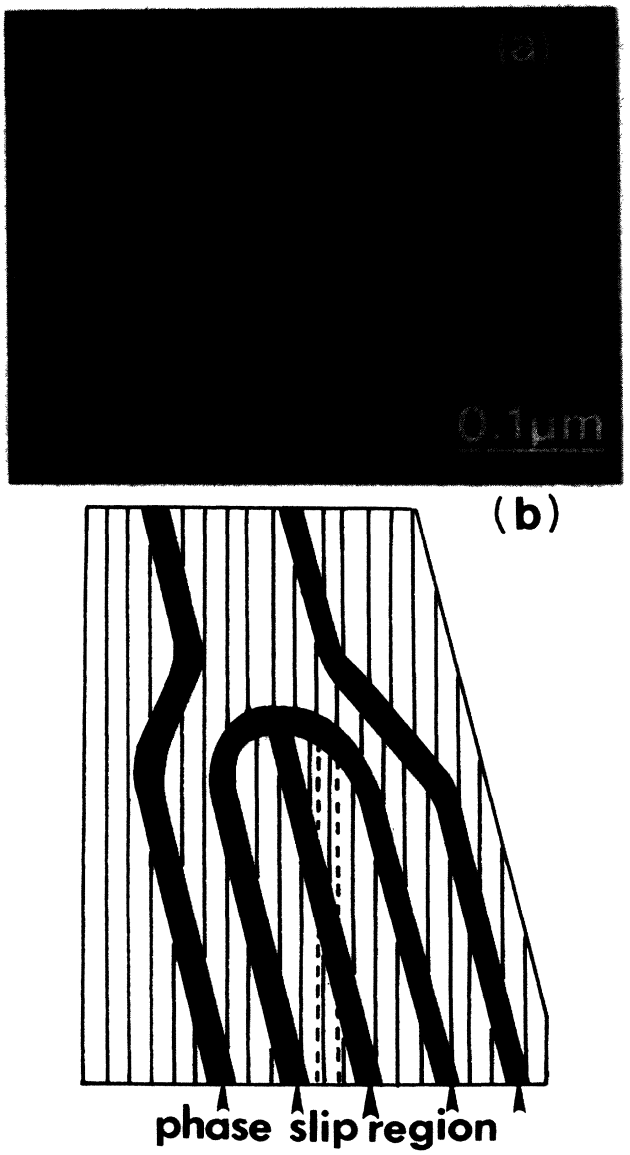

FIG. 13. Characteristic moirélike fringes where three dark fringes terminate at one point (jelly-fish pattern with three legs).

ACKNOWLEDGMENTS

The observation shown in Fig. 5 is due to Dr. Y. Fujino. We thank him for his generous offer to present his data in this paper. We also thank Dr. Y. Koyama and Mr. Z. P. Zhang for discussions and for their help in the preparation of this paper. Indeed, a major content of the Appendix is due to Dr. Koyama. Discussions and encouragement of Professor A. W. Overhauser and Professor G. L. Liedl are also greatly appreciated. The work was supported by the National Science Foundation, Solid State Chemistry Program, Grant No. DMR 8304314. In addition, the cooperation with Professor M. Hirabayashi and his group at the Research Institute for Iron, Steel, and Other Metals, Tohoku University, Sendai, Japan with respect to high-resolution electron microscopy at low temperatures under the support of the National Science Foundation, US-Japan Cooperation Program, Grant No. INT 84-12550 and of the Japan Society for the Promotion of Science was quite helpful for the progress of the present subject.

APPENDIX: THE APPEARANCE OF THE PHASE-SLIP REGION IN THE CDW LATTICE IMAGES

The appearance of the region of phase shift in the lattice images (Figs. 9 and 10) (phase-slip region) is essentially due to the contribution of split superlattice spots to the formation of lattice images and is related to the phase-slip region in the discommensuration as pointed out in the text. Here, we would like to give a theoretical support to this statement, and to the relation of the phase-slip region and the dark-field images (moirélike fringes) based on our experimental conditions. In doing so, dynamical effects are taken into account only implicitly by assuming complex amplitudes of diffracted beams at the exit surface for rather qualitative discussions.

1. Calculations of the dark-field images

First, we assume complex amplitudes for two split superlattice beams ϕ_1 and ϕ_2. Then the amplitude of the total beam ψ can be written as

$$\psi=\phi_1 e^{i(\mathbf{h}+\mathbf{H}/3-\boldsymbol{\delta})\cdot\mathbf{r}}+\phi_2 e^{i(\mathbf{h}+\mathbf{H}/3+2\boldsymbol{\delta})\cdot\mathbf{r}}$$
$$=e^{i(\mathbf{h}+\mathbf{H}/3-\boldsymbol{\delta})\cdot\mathbf{r}}\{\phi_1+\phi_2 e^{i3\boldsymbol{\delta}\cdot\mathbf{r}}\}\ . \tag{A1}$$

The complex amplitudes ϕ_1 and ϕ_2 at the exit surface are commonly calculated by the multislice method, but, because we are dealing with an incommensurate structure whose structure has not yet been well established, we proceed by simply assuming ϕ_1 and ϕ_2. Here $\mathbf{h}$ and $\mathbf{H}$ are reciprocal lattice vectors shown in Fig. 14(a) (compare this with Fig. 4) and $\boldsymbol{\delta}$ is the incommensurability defined

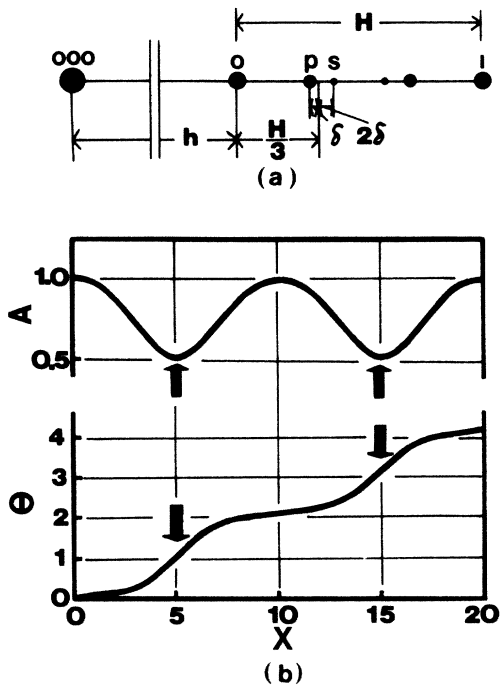

FIG. 14. (a) Schematic representation of the diffraction pattern in one of the $[h0\cdot0]^*$ directions. The figure is to explain the symbols **h** and **H** used in the Appendix. Here, the symbols 000 indicates the origin and 0 and 1 represent two fundamental diffraction spots as in Fig. 4. (b) Correspondence between the variation of intensity of the lattice images and the location of the phase-slip region.

in the text. In other words, we are superposing two split superlattice diffraction beams P and S in taking the dark-field image. The phase shift due to the lens, γ, is practically zero under the present experimental condition (diffracted beams being parallel to the axis of the lens), so that the aberration factor $e^{i\gamma}$ becomes practically one and is thus neglected.

The intensity of the beam, I, is then given by

$$I=\psi\psi^*=\phi_1\phi_1^*+\phi_2\phi_2^*+2A'\cos(3\boldsymbol{\delta}\cdot\mathbf{r}+\alpha') \ . \tag{A2}$$

Here, A' and α' are defined by

$$\phi_1^*\phi_2=A'e^{i\alpha'} \ . \tag{A3}$$

In other words, the intensity of the image (moirélike fringes) shows a sinusoidal variation of the period $1/(3\delta)$ as we mentioned in the text. Although the amplitude A' and the phase shift α' depend on actual diffraction conditions and, hence, the physical positions of the fringes are unspecified, the period itself is practically unaffected.

The contribution of higher-order harmonics, such as the fourth- and the fifth-order harmonics shown in Fig. 12 to the deviation of the intensity distribution from a sinusoidal variation and its possible relations to discommensuration problems are often discussed. These are easily taken care of by introducing the fourth- and the fifth-order harmonics with the complex amplitudes ϕ_3 and ϕ_4 into Eq. (A1). However, in the case of $TaSe_2$ in the temperature range investigated here, we notice that the intensities of P and S are especially large compared to other higher harmonics. Under this condition, we obtain approximately the same equation as Eq. (A2) unless the complex amplitude of ϕ_1 and ϕ_2 are nearly orthogonal.

2. CDW lattice images

Under the axial illumination condition with a small tilt along the active diffraction vector, the CDW lattice images are calculated by taking into the five diffraction beams or the incident beam and diffracted beams P and S on both sides of the incident beam in a symmetric fashion. Similar to subsection 1, the complex amplitude ψ is given as

$$\begin{aligned}\psi&=\phi_{000}+e^{i(\gamma-\gamma_0)}[\phi_1(e^{i(\mathbf{H}/3-\boldsymbol{\delta})\cdot\mathbf{r}}+e^{-i(\mathbf{H}/3-\boldsymbol{\delta})\cdot\mathbf{r}})+\phi_2(e^{i(\mathbf{H}/3+2\boldsymbol{\delta})\cdot\mathbf{r}}+e^{-i(\mathbf{H}/3+2\boldsymbol{\delta})\cdot\mathbf{r}})]\\&=\phi_{000}+2\phi_1e^{i(\gamma-\gamma_0)}\cos\left[\frac{\mathbf{H}}{3}-\boldsymbol{\delta}\right]\cdot\mathbf{r}+2\phi_2e^{i(\gamma-\gamma_0)}\cos\left[\frac{\mathbf{H}}{3}+2\boldsymbol{\delta}\right]\cdot\mathbf{r}\end{aligned} \tag{A4}$$

Here, ϕ_{000} indicates the complex amplitude of the incident beam. The phase factor due to the spherical aberration and the defocus, γ, and the phase shift due to the finite angles of diffracted beams, ϕ_1 and ϕ_2, with respect to the transmitted beam, ϕ_1 and ϕ_2,γ_0, have to be taken into account here.

The amplitude of the intensity variation ΔI over the background $|\phi_{000}|^2$ can be calculated based on Eq. (A4). This leads to an equation of the form (in the x direction),

$$\begin{aligned}\Delta I&=a_x\cos\left[\frac{H}{3}x\right]+b_x\sin\left[\frac{H}{3}x\right]\\&=(a_x^2+b_x^2)^{1/2}\cos\left[\frac{H}{3}x-\theta\right] \ ,\end{aligned} \tag{A5}$$

where

$$\begin{aligned}a_x&=w_0\cos(\delta x)+w_{-1}\cos(2\delta x) \ ,\\b_x&=w_0\sin(\delta x)-w_{-1}\sin(2\delta x) \ ,\\\theta&=\tan^{-1}\frac{b_x}{a_x} \ ,\\(a_x^2+b_x^2)^{1/2}&=w_0\left[1+\left[\frac{w_{-1}}{w_0}\right]^2+2\left[\frac{w_{-1}}{w_0}\right]\cos(3\delta x)\right]^{1/2}\\&=A \ ,\end{aligned} \tag{A6}$$

In deriving Eqs. (A6) and (A7), the condition

$$|\phi_{000}|\gg|\phi_1|>|\phi_2| \tag{A7}$$

is utilized. The symbols w_0 and w_{-1} are related to the amplitudes of the contributions of the first-order and the second-order harmonics (P and S) to the intensity and these are assigned as 0 and -1, because the positions of harmonics of the superlattice reflections are specified as $(H/3)-(3m+1)\delta$ with respect to the commensurate position in discommensuration theories[16,17] and, hence, $m=0$ and $m=-1$ represent P and S, respectively.

Based on Eq. (A5), the intensity of lattice images varies sinusoidary with the spacing approximately equal to $3/H$. The actual spacing is determined by the dependence of the phase shift θ on x and, depending on $d\theta/dx \gtrless 0$, the actual spacing is larger or smaller than $3/H$. The overall intensity of the lattice images is given by A in Eq. (A6) and varies periodically with the spacing $1/(3\delta)$ as the moirélike fringes, Eq. (A2). Because the lowest intensity appears at the location where the phase difference of P and S is maximum, the overall intensity variation of the lattice images coincides with that of the moirélike fringes. A qualitative relation of the intensity of the lattice images, A, and the phase shift θ as a function of x can be obtained by giving arbitrary values of δ and w's as

$$\delta=0.1\times\frac{H}{3}\ , \qquad w_{-1}/w_0=\tfrac{1}{3}\ , \tag{A8}$$

and these are plotted in Fig. 14(b). In plotting A, the value is normalized to take the value 1 at its maximum. The region where θ changes rapidly with x corresponds to the phase-slip region, and across the phase-slip region, the phase shift is equal to $2\pi/3$. In the phase-slip region, the spacing of the lattice images appears larger than other regions. The phase-slip region corresponds to the low-amplitude region and, hence, corresponds to the dark portion of the moirélike fringes. In this region, because the phase difference between the two waves P and S is maximum, the lattice images also appear less sharp in agreement with the observation.

Equation (A5) corresponds to the equation used by McMillan in his discommensuration theory.[16] Here, however, the amplitude of the cosine factors, w's, are determined by the minimization of the free-energy terms. Whether the phase-slip region in the discommensuration theory physically coincides with that of the phase-slip region of the lattice images or not is yet to be investigated, because all parameters which determine the complex amplitudes of diffracted beams are not exactly known. However, the observation of the change of the moirélike fringes to domainlike stripe patterns at lower temperatures indicates that such a real correspondence exists.[19]

*On leave of absence from the Research Institute for Iron, Steel, and other Metals, Tohoku University, Sendai, Japan, but is now back at the original address.

[1]H. Sato and R. S. Toth, Phys. Rev. **124**, 1833 (1961); **127**, 469 (1962).

[2]H. Sato and R. S. Toth, Phys. Rev. Lett. **8**, 239 (1962).

[3]H. Sato and R. S. Toth, in *Alloying Behavior in Concentrated Solid Solutions*, edited by T. B. Massalski (Gordon and Breach, New York, 1965), pp. 295–419.

[4]H. Sato and R. S. Toth, Phys. Soc. Fr. Mineral. Cristallogr. **91**, 557 (1968).

[5]M. Hirabayashi, S. Yamaguchi, K. Hiraga, N. Ino, H. Sato, and R. S. Toth, *Proceedings of the Third Bolton Landing Conference on Ordered Alloys: Structural Applications and Physical Metallurgy, 1969*, edited by B. H. Kear, C. T. Sims, N. S. Stoloff, and J. H. Westbrook (Claitor's Publishing Division, Baton Rouge, Louisiana, 1970), pp. 137–148.

[6]H. Sato, *Modulated Structures—1979 (Kailua Kona, Hawaii)*, Proceedings of the International Conference on Modulated Structures, AIP Conf. Proc. No. 53, edited by J. M. Cowley, J. B. Cohen, M. B. Salamon, and B. J. Wuensch (AIP, New York, 1979), pp. 165–167.

[7]J. A. Wilson, F. J. DiSalvo, and S. Mahajan, Adv. Phys. **24**, 117 (1975).

[8]K. K. Fung, S. McKernan, J. W. Steeds, and J. A. Wilson, J. Phys. C **14**, 5417 (1981).

[9]C. H. Chen, J. M. Gibson, and R. M. Flemming, Phys. Rev. Lett. **47**, 723 (1981).

[10]C. H. Chen, J. M. Gibson, and R. M. Flemming, Phys. Rev. B **26**, 184 (1982).

[11]J. M. Gibson, C. H. Chen, and M. L. McDonald, Phys. Rev. Lett. **50**, 1403 (1983).

[12]J. M. Gibson and M. L. McDonald, Ultramicroscopy **12**, 219 (1984).

[13]N. Otsuka and H. Sato, J. Solid State Chem. **61**, 212 (1986).

[14]D. E. Moncton, J. D. Axe, and F. J. DiSalvo, Phys. Rev. B **16**, 801 (1977).

[15]R. M. Flemming, D. E. Moncton, D. B. McWhan, and F. J. DiSalvo, Phys. Rev. Lett. **45**, 576 (1980).

[16]W. L. McMillan, Phys. Rev. B **12**, 1187 (1975); **14**, 1496 (1976).

[17]K. Nakanishi and H. Shiba, J. Phys. Soc. Jpn. **45**, 1147 (1978).

[18]B. H. Suits, S. Conturié, and C. P. Slichter, Phys. Rev. B **23**, 5142 (1981).

[19]Y. Koyama, Z. P. Zhang, and H. Sato (unpublished).

[20]Y. Fujino, H. Sato, and N. Otsuka, Proceedings of the 1985 MRS Fall Meeting, Materials Problems Solving with the Transmission Electron Microscope, edited by L. W. Hobbs, K. H. Westmacott, and D. B. Williams, 1986, Vol. 66.

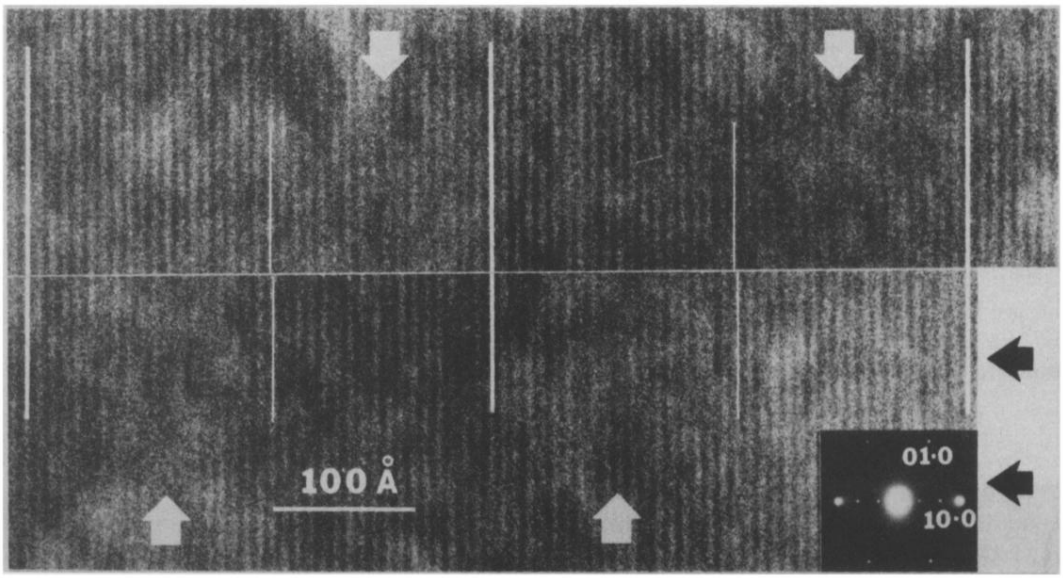

FIG. 10. Periodic change of CDW lattice spacings, showing the existence of the phase-slip region. The lower half of the picture is shifted to the left by approximately 150 Å along the solid arrows in order to compare the spacings of lattice fringes in the phase-slip region and in the other region.

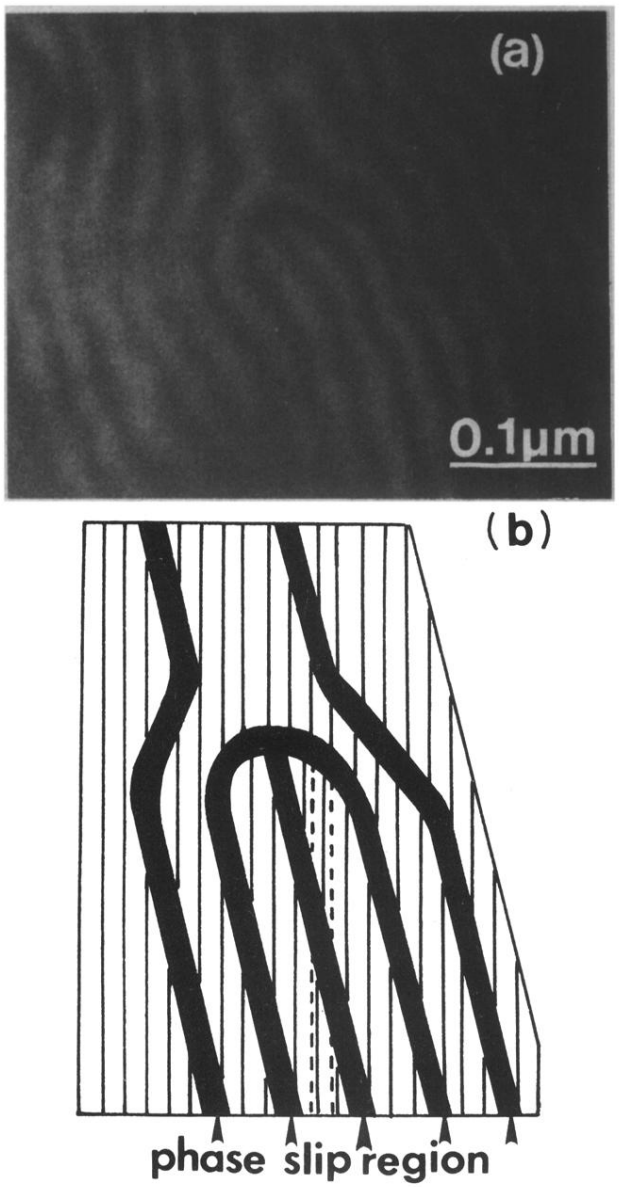

FIG. 13. Characteristic moirélike fringes where three dark fringes terminate at one point (jelly-fish pattern with three legs).

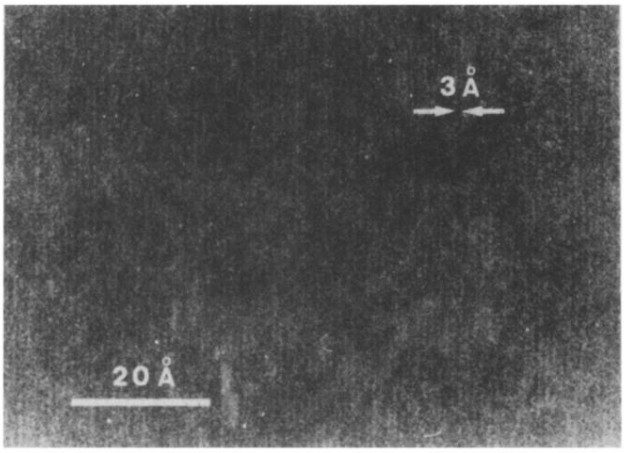

FIG. 2. High-resolution lattice images (spacing of ~ 3 Å) of the background normal structure at 97 K.

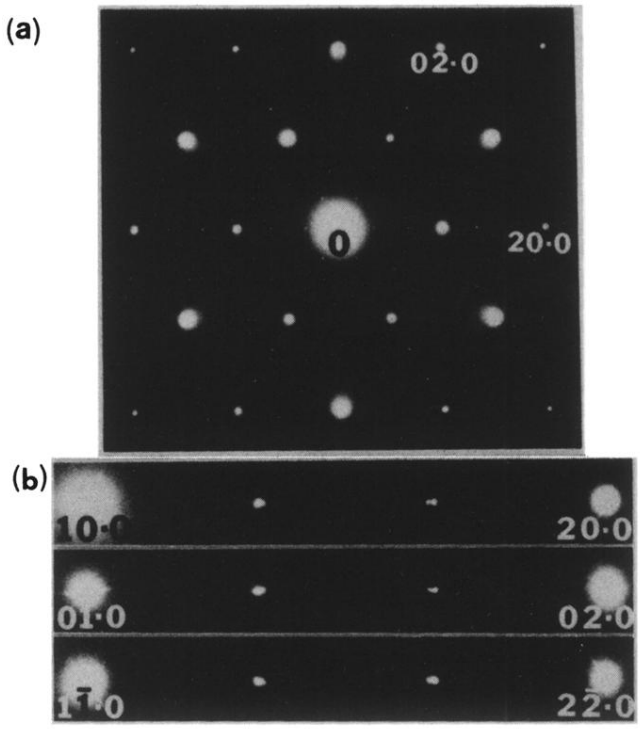

FIG. 3. (a) Electron diffraction pattern in the basal plane of $2H$-$TaSe_2$ at 97 K. The direction of the beam is parallel to the [00·1] direction. (b) Magnification of the above in three $[h\,0{\cdot}0]^*$ directions showing split superlattice spots (P and S).

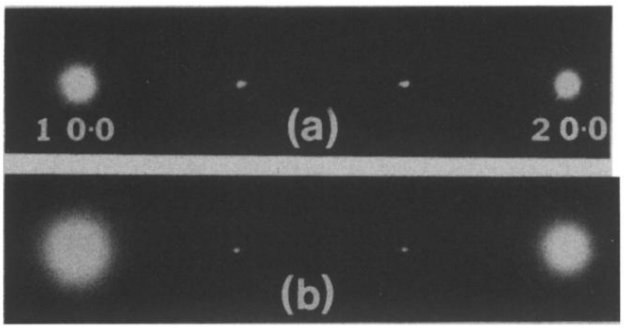

FIG. 5. Split superlattice spots at 107 K (b) as compared to those at 97 K (a). Note that S spot taken at 107 K (b) is almost invisible.

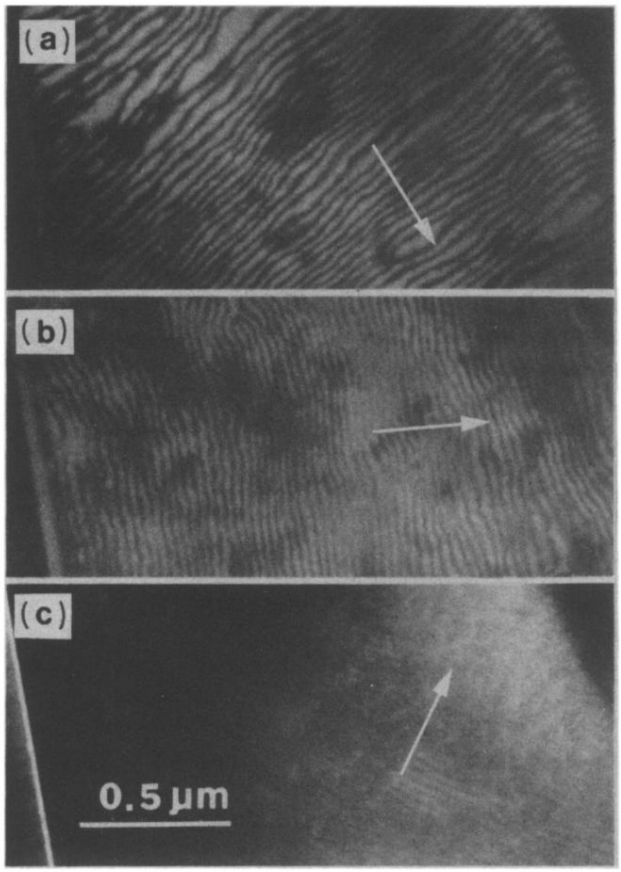

FIG. 6. Moirélike fringes obtained by the dark-field technique from the same area utilizing three different diffraction vectors, **g**, taken at 97 K. Arrows indicate the directions of **g** of each micrograph.

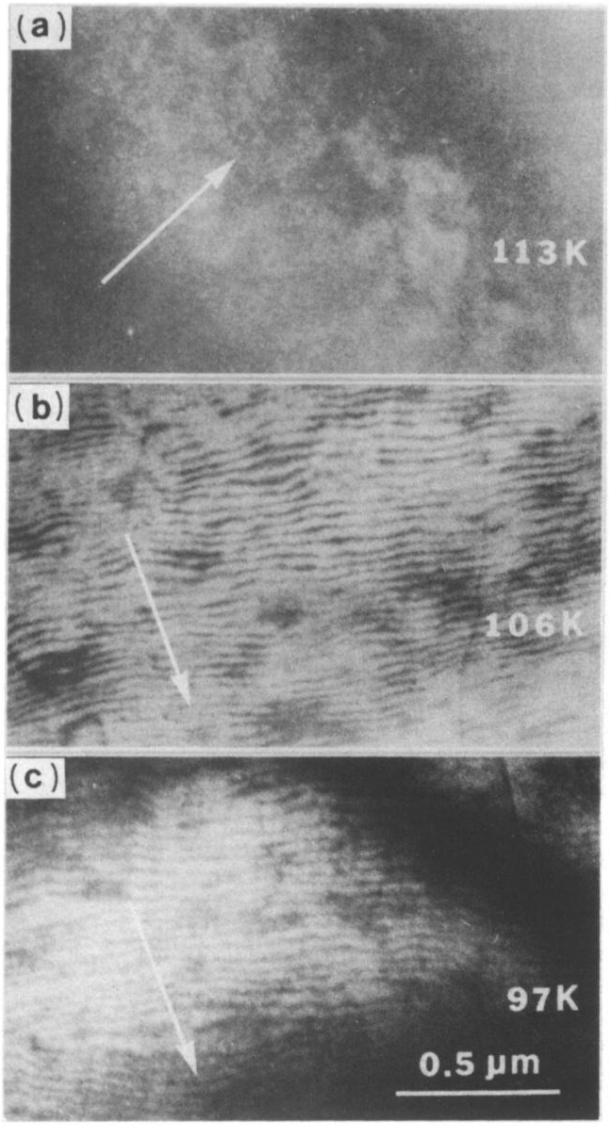

FIG. 7. Temperature dependence of the moirélike fringes. Arrows indicate the direction of the **g** vector. (a) 113 K, (b) 106 K, (c) 97 K.

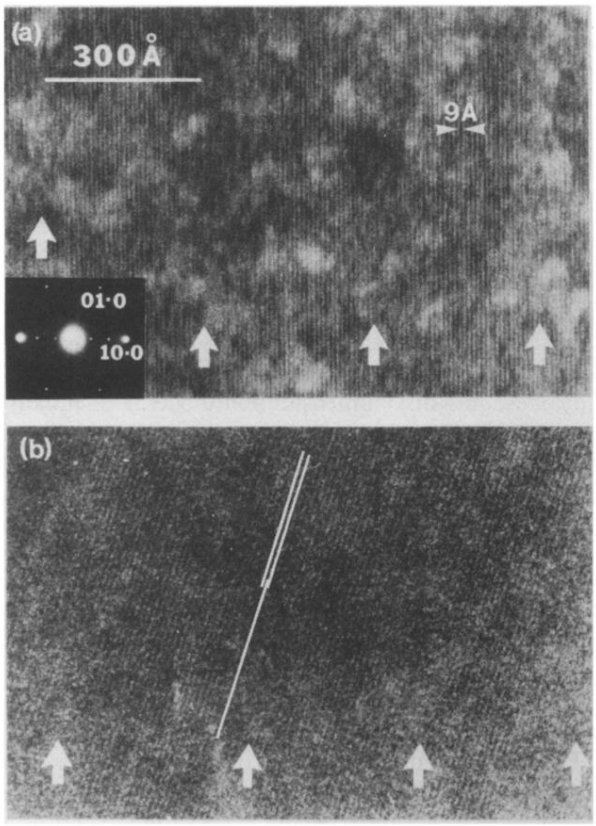

FIG. 9. High-resolution observation of CDW lattice fringes taken at 97 K. Areas of weaker contrast of lattice fringes (phase-slip region) are indicated by open arrows. (a) Lattice fringes are parallel to the phase-slip region (along with the corresponding diffraction pattern). (b) Lattice fringes are making $\sim 15°$ with respect to the phase-slip region.